

Modeling Metal Cation–Phosphate Interactions in Nucleic Acids in the Gas Phase via Alkali Metal Cation–Triethyl Phosphate Complexes

Chunhai Ruan, Hai Huang, and M. T. Rodgers*

Department of Chemistry, Wayne State University, Detroit, Michigan 48202

Received: August 10, 2007; In Final Form: October 12, 2007

Threshold collision-induced dissociation techniques are employed to determine the bond dissociation energies (BDEs) of complexes of alkali metal cations, Na^+ , K^+ , Rb^+ , and Cs^+ , to triethyl phosphate (TEP). The primary and lowest energy dissociation pathway in all cases is the endothermic loss of the neutral TEP ligand. Theoretical electronic structure calculations at the B3LYP/6-311+G(2d,2p)//B3LYP/6-31G* level of theory are used to determine the structures, molecular parameters, and theoretical estimates for the BDEs of these complexes. For the complexes to Rb^+ and Cs^+ , theoretical calculations were performed using hybrid basis sets in which the effective core potentials and valence basis sets of Hay and Wadt were used to describe the alkali metal cation, while the standard basis sets were used for all other atoms. The agreement between theory and experiment is excellent for the complexes to Na^+ and K^+ and is somewhat less satisfactory for the complexes to the heavier alkali metal cations, Rb^+ and Cs^+ , where effective core potentials were used to describe the cation. The trends in the binding energies are examined. The binding of alkali metal cations to triethyl phosphate is compared with that to trimethylphosphate.

Introduction

Nucleic acids, including DNA and RNA, are important genetic information messengers. The three steps for genetic information transfer, replication, transcription, and translation, require metals cations to mediate their activities. Metal cation–nucleic acid interactions are one of the important forces that influence the structures and mediate the functions of nucleic acids, e.g., cross-linking, degradation, stabilization (or destabilization), and mispairing.¹ There are two types of very favorable metal cation binding sites on nucleic acids, the phosphate groups and the nucleic acid bases. Alkali and alkaline earth metal cations prefer to bind to the phosphate groups along the backbone of DNA. Binding of metal cations to the phosphate groups reduces the repulsion between the neighboring negatively charged nucleotide units and therefore helps stabilize the structure of nucleic acids. For example, Mg^{2+} binding is found to stabilize the structure and increase the melting temperature of DNA.² Experimental evidence from NMR,^{3–5} X-ray crystallography,^{6,7} and molecular dynamics simulations^{8,9} indicates that biologically important cations, Na^+ , K^+ , Mg^{2+} , and Ca^{2+} , interact with B-form DNA in a sequence-specific manner and therefore stabilize specific DNA sequences. Monovalent cations may compete with water and partially (10–30%) replace water molecules in the minor groove of the B-form DNA.¹⁰ The locations of monovalent cations appear to be influenced by the nucleic acid bases present, backbone functional groups, and electrostatic interactions.¹⁰ Metal cations may also bind to the heteroatoms of the nucleic acid bases, which usually leads to destabilization of nucleic acid structures.¹¹

The phosphate groups along the backbone of nucleic acids are important binding sites for alkali and alkaline earth metal cations. Schneider, et al.^{12,13} studied the distribution of five metal cations (Na^+ , Mg^{2+} , K^+ , Ca^{2+} , and Zn^{2+}) and water around a

deprotonated phosphate group from X-ray crystal structures and ab initio calculations. The 178 crystal structures suggest that these cations prefer asymmetric monodentate binding over symmetric bidentate binding to the phosphate group. In contrast, their theoretical calculations suggest that bidentate binding of these metal cations to an isolated phosphate group is preferred, but the presence of even a single water molecule alters this preference such that an asymmetric monodentate binding interaction to the phosphate group becomes more favorable. Similar results were obtained for ab initio calculations of hydrated Mg^{2+} and Ca^{2+} with deprotonated dimethyl phosphate where the cations were found to prefer monodentate binding.¹⁴ This preference for monodentate binding is due to mutual interactions between the cation, phosphate group, and water molecules. The monodentate binding observed in the crystal structures likely arises from interactions with water molecules that are present in the crystals.

To better understand how cation binding influences the structure and stability of phosphate esters, we have undertaken systematic studies aimed at the characterization of the structures, cation binding affinities, and activation propensities of a wide variety of metal cation–phosphate ester complexes. The influence of the size, charge, and valence electronic structure of the metal cation on the binding and activation propensities is being investigated by including main group metal (Li, Na, K, Rb, Cs, Mg, and Al) and transition metal (Sc, Ti, V, Cr, Mn, Fe, Co, Ni, Cu, and Zn) cations in their +1 and +2 oxidation states as appropriate in our studies. The influence of the size, number, and nature of the alkyl groups, the presence of acidic hydrogen atoms, and the charge (neutral versus deprotonated) of the phosphate ester have upon the binding and activation propensities is being examined by including mono-, di-, and trimethyl phosphate, mono-, di-, and triethyl phosphate, and mono- and di-isopropyl phosphate in our work. In our first such published study, we examined the interactions of alkali metal cations Li^+ , Na^+ , K^+ , Rb^+ , and Cs^+ with trimethyl phosphate (TMP),

* To whom correspondence should be addressed. Phone: 313-577-2431; e-mail: mrogers@chem.wayne.edu.

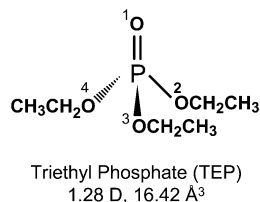


Figure 1. Structure of triethyl phosphate (TEP). The B3LYP/6-311+G-(2d,2p) dipole moment and PBE0/6-311+G(2d,2p) isotropic molecular polarizability calculated here are also shown.

determined the preferred modes of binding, and measured and calculated the alkali metal cation affinities of TMP.¹⁵

There are several favorable metal cation binding sites on nucleic acids: the nucleic acid bases, the phosphate groups, and the sugar rings. Metal cation binding significantly influences the physical properties, conformation, and functionality of nucleic acids. Thus, the results of these studies coupled with complementary studies of metal cation binding to nucleic acid bases and sugars should allow rational prediction of the preferred metal cation binding sites to nucleic acids and control over the reactivity and dissociation characteristics of metal cation–nucleic acid complexes.

In the present study, our metal cation–phosphate ester studies are expanded to include complexes of alkali metal cations to triethyl phosphate (TEP, Figure 1). In particular, triethyl phosphate is chosen for study as it is a good model for the 5'-phosphate ester linkage in nucleic acids. The kinetic energy dependences of the collision-induced dissociation (CID) of alkali metal cation-TEP complexes, $M^+(\text{TEP})$, where $M^+ = \text{Na}^+, \text{K}^+, \text{Rb}^+, \text{and Cs}^+$, with Xe are examined using a guided ion beam tandem mass spectrometer. The cross sections for the primary CID processes observed for each complex are analyzed using methods previously developed.¹⁶ The trends in the binding energies of alkali metal cations to TEP are examined. The binding of alkali metal cations to TEP is compared with that to TMP.

Experimental Section

General Procedures. Cross sections for CID of $M^+(\text{TEP})$, where $M^+ = \text{Na}^+, \text{K}^+, \text{Rb}^+, \text{and Cs}^+$, are measured using a guided ion beam tandem mass spectrometer that has been described in detail previously.¹⁷ Metal cations are generated in a continuous dc discharge by argon ion sputtering of a cathode with a cavity containing the alkali metal (Na and K) or chloride salt of the alkali metal cation of interest (RbCl and CsCl). Typical operating conditions of the discharge are 0.5–4.0 kV and 5–40 mA for alkali metal cation production in a flow of roughly 10% argon in helium. The complexes are generated in a flow tube ion source by condensation of the alkali metal cation and neutral TEP molecule. These complexes are collisionally stabilized and thermalized by in excess of 10^5 collisions with the He and Ar bath gases such that the internal energies of the ions emanating from the source region are believed to be well-described by a Maxwell–Boltzmann distribution at room temperature. The ions are effusively sampled from the source, focused, accelerated, and focused into a magnetic sector momentum analyzer for mass analysis. Mass-selected ions are decelerated to a desired kinetic energy and focused into an octopole ion beam guide. The octopole passes through a static gas cell containing Xe at low pressure (0.05–0.20 mTorr) to ensure that multiple ion–neutral collisions are improbable. The octopole ion guide acts as an efficient trap for ions in the radial direction. Therefore, loss of scattered reactant and product ions

in the octopole region is almost entirely eliminated.^{18–20} Xe is used here and in general for all of our CID measurements because it is heavy and polarizable and therefore leads to more efficient kinetic to internal energy transfer in the CID process.^{21–23} Product and remaining reactant ions drift to the end of the octopole, where they are focused into a quadrupole mass filter for mass analysis and subsequently detected with a secondary electron scintillation detector and standard pulse counting techniques.

Ion intensities are converted to absolute cross sections using a Beers' law analysis as described previously.²⁴ Absolute uncertainties in cross section magnitudes are estimated to be $\pm 20\%$, which are largely the result of errors in the pressure measurement and the length of the interaction region. Relative uncertainties are approximately $\pm 5\%$.

Ion kinetic energies in the laboratory frame, E_{lab} , are converted to energies in the center of mass frame, E_{CM} , using the formula $E_{\text{CM}} = E_{\text{lab}}m/(m + M)$, where M and m are the masses of the ionic ($M^+(\text{TEP})$) and neutral (Xe) reactants, respectively. All energies reported below are in the center-of-mass frame unless otherwise noted. The absolute zero and distribution of the ion kinetic energies are determined using the octopole ion guide as a retarding potential analyzer as previously described.²⁴ The distribution of ion kinetic energies is nearly Gaussian with a full width at half maximum (fwhm) between 0.2 and 0.4 eV (lab) for these experiments. The uncertainty in the absolute energy scale is ± 0.05 eV (lab).

Pressure-dependent studies of all CID cross sections examined here were performed because multiple collisions can influence the shape of CID cross sections, and the threshold regions are most sensitive to these effects. Data free from pressure effects are obtained by extrapolating to zero reactant pressure, as described previously.²⁵ Thus, cross sections subjected to thermochemical analysis are the result of single bimolecular encounters.

Quantum Chemical Calculations. To obtain model structures, vibrational frequencies, and energetics for neutral TEP and the $M^+(\text{TEP})$ complexes, simulated annealing and quantum chemical calculations were performed using HyperChem and Gaussian 03.²⁶ One hundred cycles of simulated annealing were performed to find reasonable candidates for the ground-state structures. Geometry optimizations and frequency analyses were performed at the B3LYP/6-31G* level for all plausible low-energy neutral TEP and $M^+(\text{TEP})$ candidate structures. For the Rb^+ and Cs^+ complexes, geometry optimizations and frequency analyses were performed using a hybrid basis set in which the effective core potentials (ECPs) and valence basis sets of Hay and Wadt were used to describe the alkali metal cation,²⁷ while the all-electron 6-31G* basis sets were used for the C, H, O, and P atoms. As suggested by Glendening et al.,²⁸ a single polarization (d) function was added to the Hay–Wadt valence basis set for Rb and Cs, with exponents of 0.24 and 0.19, respectively. The calculated vibrational frequencies were scaled by a factor of 0.9804 and are listed in Table 1S of the Supporting Information. Table 2S lists the rotational constants for the ground-state conformations. Single-point energy calculations at the B3LYP/6-311+G(2d,2p) and B3LYP/6-311+G(2d,2p), HW levels of theory were performed using the B3LYP/6-31G* and B3LYP/6-31G*, HW optimized geometries. To obtain accurate energetics, zero-point energy (ZPE) and basis set superposition error (BSSE) corrections were included in the calculation of theoretical BDEs.^{29,30} Ground-state structures were determined by comparing the absolute energies of the low-energy conformers of neutral TEP and the $M^+(\text{TEP})$ complexes.

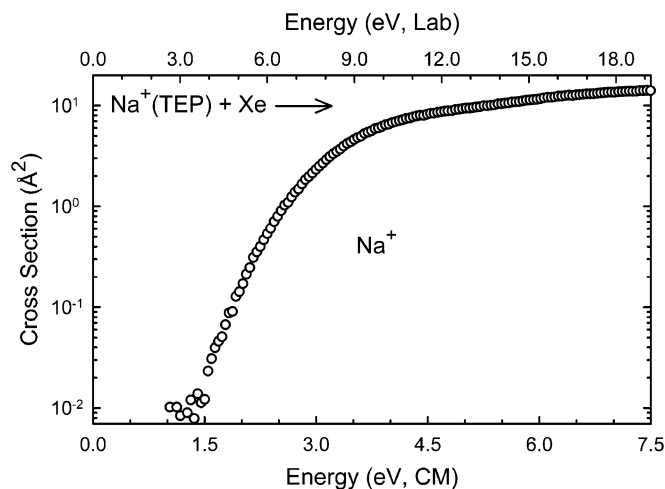


Figure 2. Cross sections for the collision-induced dissociation of $\text{Na}^+(\text{TEP})$ with Xe as a function of collision energy in the center-of-mass frame (lower x -axis) and laboratory frame (upper x -axis). Data are shown for a Xe pressure of 0.2 mTorr.

The polarizability of the ligand is one of the key factors that influence the strength of metal–ligand binding. A theoretical calculation of the isotropic molecular polarizability of TEP based on a dipole electric field was carried out at the PBE0/6-311+G-(2d,2p) level of theory. This level of theory was chosen because it has been shown to provide polarizabilities that are in better agreement with experimental values than polarizabilities computed using the B3LYP functional that is used here for the structures and energetics of these systems.³¹ The polarizability of the TEP ligand is one of the molecular parameters used for the thermochemical analysis of experimental data.

Thermochemical Analysis. The threshold regions of the CID cross sections are modeled using eq 1

$$\sigma(E) = \sigma_0 \sum_i g_i (E + E_i - E_0)^n / E \quad (1)$$

where σ_0 is an energy-independent scaling factor, E is the relative translational energy of the reactants, E_0 is the threshold for reaction of the ground electronic and ro-vibrational state, and n is an adjustable parameter that describes the efficiency of kinetic to internal energy transfer.³² The summation is over the ro-vibrational states of the reactant $\text{M}^+(\text{TEP})$ complexes, i , where E_i is the excitation energy of each ro-vibrational state, and g_i is the population of those states ($\sum g_i = 1$).

The Beyer–Swinehart algorithm is used to evaluate the density of ro-vibrational states,^{33–35} and the relative populations, g_i , are calculated as a Maxwell–Boltzmann distribution at 298 K, the internal temperature of the reactants. The average internal energies at 298 K of neutral TEP and the $\text{M}^+(\text{TEP})$ complexes are also given in Table 1S. We have estimated the sensitivity of our analysis to the deviations from the true frequencies by scaling the vibrational frequencies (prescaled by 0.9804) by $\pm 10\%$. The corresponding change in the average vibrational energy is taken to be an estimate of one standard deviation of the uncertainty in the vibrational energy (Table 1S) and is included in the uncertainties listed with the threshold energies.

We also consider the possibility that the collisionally activated complex ions do not dissociate on the time scale of the experiment ($\sim 10^{-4}$ s) by including statistical theories for unimolecular dissociation, specifically Rice–Ramsperger–Kassel–Marcus (RRKM) theory, into eq 1 as described in detail elsewhere.^{16,36} The ro-vibrational frequencies appropriate for the energized molecules and the transition states (TSs) leading to

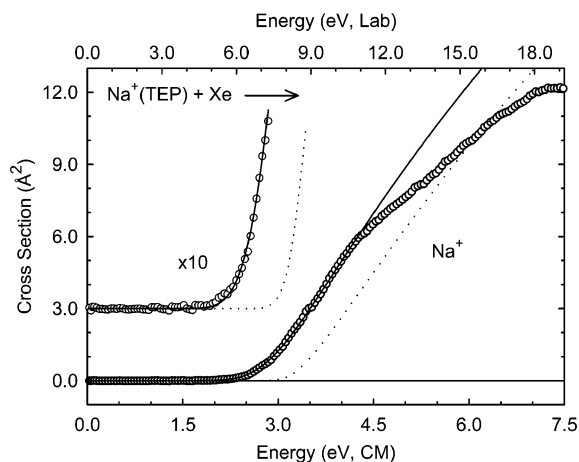


Figure 3. Zero-pressure-extrapolated cross sections for collision-induced dissociation of $\text{Na}^+(\text{TEP})$ with Xe in the threshold region as a function of kinetic energy in the center-of-mass frame (lower x -axis) and laboratory frame (upper x -axis). The solid lines show the best fit to the data using eq 1 convoluted over the neutral and ion kinetic and internal energy distributions. The dotted lines show the model cross sections in the absence of experimental kinetic energy broadening for reactants with an internal energy corresponding to 0 K.

dissociation are given in Tables 1S and 2S, where we assume that the TSs are loose and product-like because the interaction between the alkali metal cation and TEP ligand is largely electrostatic. The TS vibrations used are the frequencies corresponding to the neutral product, TEP. The transitional frequencies, those that become rotations of the completely dissociated products, are treated as rotors corresponding to a phase space limit (PSL) as described in detail elsewhere.¹⁶ The TS is variationally located at the centrifugal barrier, which is dependent upon the polarizability of the neutral TEP ligand.

The model represented by eq 1 is expected to be appropriate for translationally driven reactions³⁷ and has been shown to reproduce CID cross sections well. The model of eq 1 is convoluted with the kinetic energy distributions of the $\text{M}^+(\text{TEP})$ and Xe reactants, and a nonlinear least-squares analysis of the data is performed to give optimized values for the parameters σ_0 , E_0 or $E_0(\text{PSL})$, and n . The errors associated with the measurement of E_0 or $E_0(\text{PSL})$ are estimated from the range of threshold values determined for the zero-pressure-extrapolated data sets, the variations associated with uncertainties in the vibrational frequencies (scaling as described above), and the error in the absolute energy scale, 0.05 eV (lab). For analyses that include the RRKM lifetime analysis, the uncertainties in the reported $E_0(\text{PSL})$ values also include the effects of increasing and decreasing the time assumed available for dissociation ($\sim 10^{-4}$ s) by a factor of 2.

Equation 1 explicitly includes the internal energy of the ion, E_i . All energy available is treated statistically because the ro-vibrational energy of the reactants is redistributed throughout the ion upon impact with Xe. Because the CID processes examined here are simple noncovalent bond cleavage reactions, the $E_0(\text{PSL})$ values determined by analysis with eq 1 can be equated to 0 K BDEs.^{38,39}

Results

Cross Sections for Collision-Induced Dissociation. Experimental cross sections were obtained for the interaction of Xe with four $\text{M}^+(\text{TEP})$ complexes, where $\text{M}^+ = \text{Na}^+, \text{K}^+, \text{Rb}^+, \text{and Cs}^+$. Figure 2 shows data for the $\text{Na}^+(\text{TEP})$ complex. Similar behavior is observed for the other $\text{M}^+(\text{TEP})$ complexes;

TABLE 1: Fitting Parameters of Eq 1, Threshold Dissociation Energies at 0 K, and Entropies of Activation at 1000 K of M⁺(TEP)^a

species	σ_0	n	E_0^b (eV)	E_0 (PSL) (eV)	kinetic shift (eV)	ΔS^\ddagger (PSL) (J mol ⁻¹ K ⁻¹)
Na ⁺ (TEP)	13.3 (0.9)	1.4 (0.1)	3.00 (0.06)	1.88 (0.08)	1.12	34 (2)
K ⁺ (TEP)	28.4 (3.0)	1.2 (0.1)	2.06 (0.07)	1.40 (0.06)	0.66	23 (3)
Rb ⁺ (TEP)	4.2 (0.3)	1.1 (0.1)	1.99 (0.04)	1.35 (0.05)	0.64	22 (2)
Cs ⁺ (TEP)	7.4 (0.7)	1.2 (0.1)	1.84 (0.06)	1.25 (0.05)	0.59	14 (2)

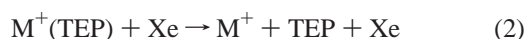
^a Uncertainties are listed in parentheses. Average values for loose PSL transition state, except as noted. ^b No RRKM analysis.

TABLE 2: Geometrical Parameters of Ground-State B3LYP/6-31G* and B3LYP/6-31G*, HW Optimized Structures of TEP and M⁺(TEP) Complexes

species	M ⁺ –O1 (Å)	M ⁺ –O2 (Å)	P=O1 (Å)	P–O2 (Å)	P–OX (Å) ^a	C–OX (Å) ^b	\angle M ⁺ O1PO2 (°)
TEP			1.482	1.607	1.607	1.450	
Na ⁺ (TEP)	2.181	2.488	1.500	1.622	1.582	1.475	–6.0
K ⁺ (TEP)	2.461	4.258	1.499	1.590	1.592	1.464	–24.5
Rb ⁺ (TEP)	2.697	4.349	1.496	1.595	1.595	1.461	–18.8
Cs ⁺ (TEP)	2.922	4.574	1.494	1.592	1.599	1.460	–28.6

^a Average values for the P–O3 bond and P–O4 bond lengths. ^b Average values for the C–O2, C–O3, and C–O4 bond lengths.

data for these systems is shown in Figure 1S of the Supporting Information. Over the collision energy range studied, two types of processes are observed: loss of the intact TEP ligand and ligand exchange with Xe as summarized in reactions 2 and 3.



In all cases, the most favorable pathway is the loss of the neutral TEP ligand. Ligand exchange to form M⁺Xe is observed only for the K⁺(TEP) complex. It is likely that the analogous ligand exchange processes occur for all complexes but that the signal intensities for the Me⁺Xe product in the other experiments were not sufficient to differentiate it from background noise.

Threshold Analysis. The model of eq 1 was used to analyze the thresholds for reaction 2 in four M⁺(TEP) systems. The results of these analyses are provided in Table 1. A fit to the Na⁺ CID product cross section for the Na⁺(TEP) complex is shown in Figure 3. Fits to the M⁺ CID product cross sections for the other M⁺(TEP) complexes are shown in Figure 2S of the Supporting Information. In all cases, the experimental cross sections for CID reaction 2 are accurately reproduced using a loose PSL TS model.¹⁶ Previous work has shown that this model provides the most accurate assessment of the kinetic shifts for CID processes of electrostatically bound ion–molecule complexes.^{16,17} Good reproduction of the data is obtained over energy ranges exceeding 3.0 eV and cross section magnitudes of at least a factor of 100. Table 1 also lists threshold values, E_0 , obtained without including the RRKM lifetime analysis. Comparison of these values with the E_0 (PSL) values determined including the RRKM lifetime analysis provides estimates for the kinetic shifts associated with the finite experimental time scale that vary from 0.59 to 1.12 eV across these systems. The number of vibrational frequencies is the same, 75, for all of these M⁺(TEP) complexes. Because the density of states of the complex at threshold depends on the measured BDE, the kinetic shifts are expected to correlate with the BDEs. As expected, the kinetic shifts correlate directly with the measured threshold energies, Table 1.

The entropy of activation, ΔS^\ddagger , is a measure of the looseness of the TS and also a reflection of the complexity of the system. It is largely determined by the molecular parameters used to model the energized molecule and the TS for dissociation but also depends on the threshold energy. The ΔS^\ddagger (PSL) values at 1000 K are listed in Table 1 and decrease from 34 to 14 J/K·

mol as the size of the metal cation increases and the strength of the M⁺–TEP binding interaction decreases from Na⁺ to Cs⁺.

Theoretical Results. Theoretical structures for neutral TEP and the M⁺(TEP) complexes were calculated as described above. Table 2 provides key geometrical parameters of the optimized geometries for the ground-state conformers of each of these species. The geometry-optimized structures for neutral TEP and the M⁺(TEP) complexes are shown in Figure 4 and 5, respectively. The Cartesian coordinates of the geometry-optimized structures for all ground-state species are given in Table 3S of the Supporting Information.

Neutral TEP Ligand. Several representative low-energy conformers were found for neutral TEP and are shown in Figure 4. In the ground-state structure, the three ethyl groups are completely staggered to minimize repulsion with each other. Rotation of a single ethyl group away from the oxo oxygen increases the energy by 4.9 kJ/mol, while rotation of a single ethyl group toward the oxo oxygen increases the energy by 5.6 kJ/mol. Rotation of additional ethyl groups leads to even higher energy configurations. For example, the stability decreases by 10.2 kJ/mol (relative to the ground-state conformer) when one ethyl group is rotated toward the oxo oxygen atom, while another ethyl group is rotated away from the oxo oxygen atom. The dipole moment and isotropic molecular polarizability of the ground-state conformer are found to be 1.28 D and 16.42 Å³, respectively (Figure 1).

M⁺(TEP) Complexes. Several representative low-energy conformers of each of the M⁺(TEP) complexes were found and are shown in Figure 5 for the Na⁺(TEP) complex. For all of the M⁺(TEP) complexes, the ground-state structure involves bidentate interaction of the alkali metal cation with the oxo oxygen atom and one of the alkoxy oxygen atoms. One of the ethyl groups is oriented away from the oxo oxygen to minimize repulsion with M⁺, while the other two ethyl groups remain staggered to minimize repulsion with each other. This presumably occurs so that metal cation gains additional stabilization by interacting with the alkoxy oxygen atom. Rotation of one ethyl group away from the metal cation results in a configuration in which the metal cation only interacts with the oxo oxygen atom. Loss of the interaction with the alkoxy oxygen atom costs 11.8 kJ/mol for the Na⁺(TEP) complex. This indicates that interaction with the alkoxy oxygen atom enhances the binding by ~10%. Such bidentate binding is likely to provide a similar amount of relative stabilization for all of these M⁺(TEP) complexes.

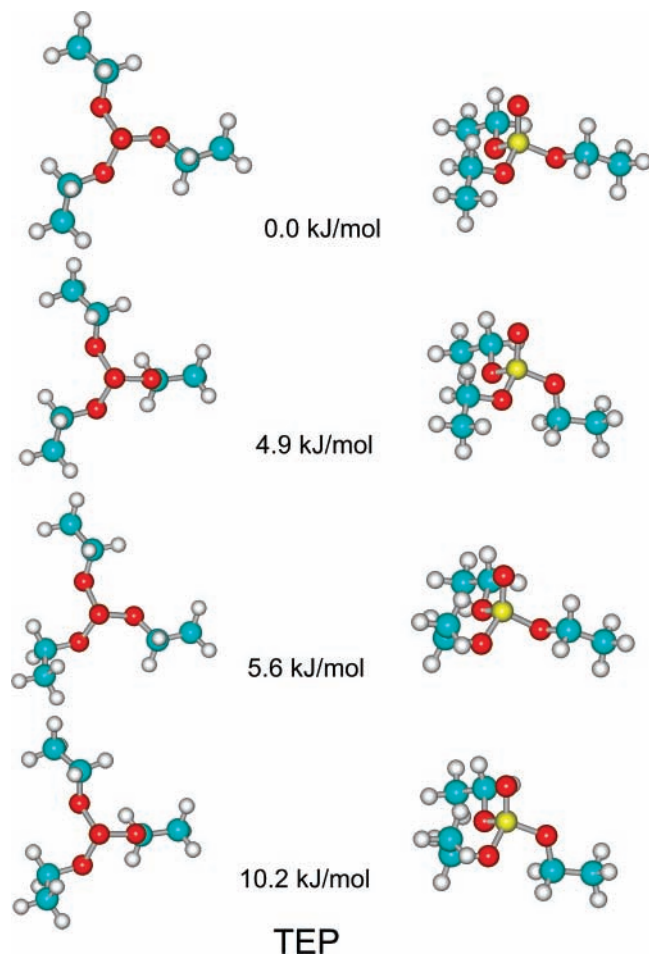


Figure 4. B3LYP/6-31G* optimized geometries of triethyl phosphate (TEP). Two views of each structure and B3LYP/6-311+G(2d,2p) relative stabilities are shown.

The ground-state structures of all of the $M^+(\text{TEP})$ complexes are very similar. The metal cation–oxo oxygen ($M^+-\text{O1}$) bond length is significantly shorter than the metal cation–alkoxy oxygen ($M^+-\text{O2}$) bond length for all complexes. The $M^+-\text{O1}$ and $M^+-\text{O2}$ bond lengths are found to increase from 2.181 Å to 2.922 Å and from 2.488 Å to 4.574 Å, respectively, as the size of alkali metal cation increases from Na^+ to Cs^+ . In contrast, the $M^+(\text{TEP})$ BDE decreases from 179.7 kJ/mol to 98.1 kJ/mol as the size of the alkali metal cation increases. Upon Na^+ binding to TEP, the $\text{P}=\text{O1}$, $\text{P}-\text{O2}$, and $\text{C}-\text{O}$ bonds are lengthened, while the $\text{P}-\text{O3}$ and $\text{P}-\text{O4}$ bonds become somewhat shorter. In contrast, for all of the other alkali metal cations, the $\text{P}=\text{O1}$ and $\text{C}-\text{O}$ bonds are lengthened, while the $\text{P}-\text{O2}$, $\text{P}-\text{O3}$, and $\text{P}-\text{O4}$ bond lengths decrease. The $\text{C}-\text{C}$ and $\text{C}-\text{H}$ bonds are essentially unaffected by alkali metal cation binding for all complexes. The change in the $\text{C}-\text{O}$ bond lengths is largest for the Na^+ complex and decreases from 0.025 to 0.010 Å as the size of alkali metal cation increases. The alkali metal cations are shifted away from the two alkoxy oxygen atoms not in directly interacting with the metal cation such that the $\angle M^+\text{O1PO2}$ dihedral angle is small and varies from -6.0° to -28.6° as the size of alkali metal cation increases.

Discussion

Trends in the Binding of Alkali Metal Cations to TEP.

The 0 K BDEs of the $M^+(\text{TEP})$ complexes measured and computed here are summarized in Table 3. The variation in the measured BDEs with the size of the alkali metal cation is shown

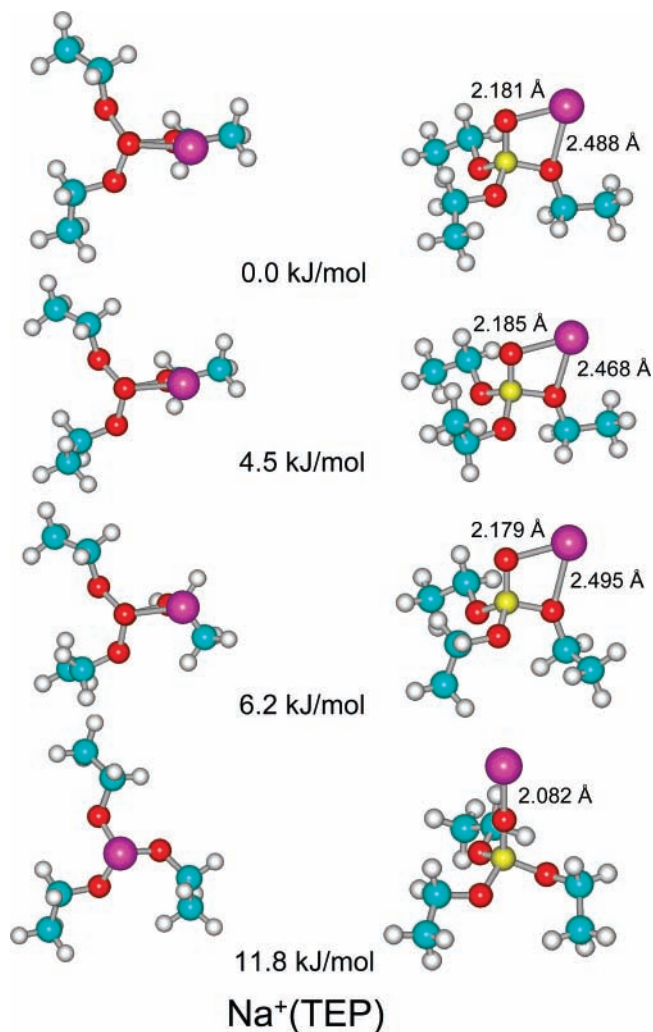


Figure 5. B3LYP/6-31G* optimized geometries of the $\text{Na}^+(\text{TEP})$ complexes. Two views of each structure and B3LYP/6-311+G(2d,2p) relative stabilities are shown.

in Figure 6. As can be seen in the figure, the $M^+(\text{TEP})$ BDEs are found to decrease monotonically as the size of alkali metal cation increases from Na^+ to Cs^+ . This can be explained in terms of the electrostatic interactions that control the binding in these complexes. The alkali metal cations have s^0 electron configurations and spherically symmetric electron densities. The alkali metal cation–ligand bond lengths are mainly determined by the size of the cation, such that the larger the cation radius the longer the bond distance and the weaker the interaction. As a result of the relatively weak and purely electrostatic binding in these $M^+(\text{TEP})$ complexes, no activated dissociation of TEP was observed upon alkali metal cation binding, suggesting that activation of the TEP may require either stronger binding or specific orbital interactions between the metal cation and the TEP ligand.

Comparison of Theory and Experiment. The $M^+(\text{TEP})$ BDEs at 0 K were calculated at the B3LYP/6-311+G(2d,2p)//B3LYP/6-31G* and B3LYP/6-311+G(2d,2p), HW//B3LYP/6-31G*, HW levels of theory including ZPE and BSSE corrections. The theoretical BDEs of the $M^+(\text{TEP})$ complexes are summarized in Table 3 along with the measured values. The agreement between theory and experiment is illustrated in Figure 7. Excellent agreement between the theoretical and the TCID experimental results is obtained for the $\text{Na}^+(\text{TEP})$ and $\text{K}^+(\text{TEP})$ complexes. In contrast, theory underestimates the strength of binding to Rb^+ and Cs^+ . The mean absolute deviation (MAD)

TABLE 3: Enthalpies of Alkali Metal Cation Binding to TEP at 0 K in kJ/mol

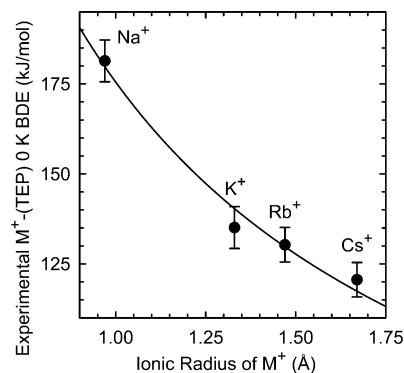
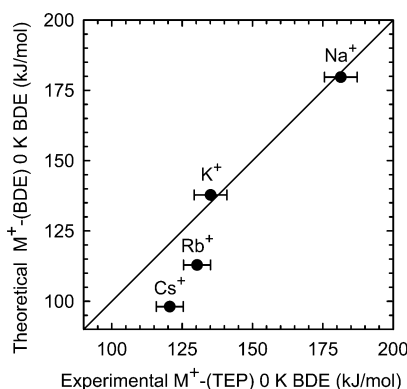
M ⁺	experiment (TCID) ^a		theory		
	TEP ^b	TMP ^c	D _e ^d	D ₀ ^{d,e}	D _{0,BSSE} ^{d,f}
Na ⁺	181.4 (5.8)	171.7 (5.8)	186.6	183.7	179.7
K ⁺	135.1 (5.8)	135.1 (3.9)	141.1	139.2	137.8
Rb ⁺	130.3 (4.8)	123.5 (5.8)	115.0	113.8	112.9
Cs ⁺	120.6 (4.8)	103.2 (3.9)	100.7	99.4	98.1

^a Threshold collision-induced dissociation. Uncertainties are listed in parentheses. ^b Present results. ^c Ref 15. ^d Calculated at the B3LYP/6-311+G(2d,2p)//B3LYP/6-31G* and B3LYP/6-311+G(2d,2p),HW//B3LYP/6-31G*,HW. ^e Including ZPE corrections with B3LYP/6-31G* and B3LYP/6-31G*,HW frequencies scaled by 0.9804. ^f Also includes BSSE corrections.

between theory and experiment for all four complexes is 11.1 ± 10.5 kJ/mol, almost twice as large as the average experimental uncertainty (AEU), 5.3 ± 0.6 kJ/mol. The experimental results of Rb⁺ and Cs⁺ complexes in particular exhibit less satisfactory agreement with theory, which is likely the result of the effective core potentials used to describe these two cations and which provides the dominant contributions to the MAD. If the Rb⁺-(TEP) and Cs⁺-(TEP) complexes are not included, the MAD decreases to 2.2 ± 0.7 kJ/mol. Similar deviations between the measured and calculated BDEs for other Rb⁺(ligand) and Cs⁺-(ligand) complexes we previously investigated have been found.^{15,40–47} For BDEs computed at the MP2(full)/6-311+G(2d,2p)//B3LYP/6-31G* and B3LYP/6-311+G(2d,2p)//B3LYP/6-31G* levels of theory, the MADs are 6.3 ± 5.5 kJ/mol and 19.0 ± 4.0 kJ/mol, respectively. Thus, the results found here are not surprising. Indeed, calculations at MP2(full) level of theory would clearly provide better results but were not pursued as a result of the size of these systems.

Conversion from 0 to 298 K. The 0 K BDEs determined here are converted to 298 K bond enthalpies and free energies to allow comparison to literature values and to commonly employed experimental conditions. The conversions are calculated using standard formulas (assuming harmonic oscillator and rigid rotor models) and the vibrational and rotational constants determined for the B3LYP/6-31G* and B3LYP/6-31G*, HW optimized geometries, listed in Tables 1S and 2S. Table 4S lists the 0 and 298 K enthalpy, free energy, and enthalpic and entropic corrections for all M⁺(TEP) complexes experimentally and theoretically determined (from Table 3). Uncertainties are determined by 10% variation in the molecular constants.

Comparison of Alkali Metal Cation Binding to TEP and TMP. The mode of alkali metal cation binding determined for the M⁺(TEP) complexes is very similar to that found for the analogous M⁺(TMP) complexes.¹⁵ The most favorable binding geometries involve bidentate interaction of the alkali metal cation with the phosphate ester, in which the metal cation interacts with the lone pairs of electrons from both the oxo oxygen atom and one of the alkoxy oxygen atoms. To facilitate the bidentate interaction, the ethyl group rotates away from the metal cation. However, a small difference in the ground-state geometries for Na⁺ binding to TEP and TMP is found. In the ground-state structure of Na⁺(TEP), the M⁺-O1 and M⁺-O2 bond lengths are somewhat similar and differ by only 0.307 Å. In contrast, the analogous conformation for Na⁺(TMP) (where the M⁺-O1 and M⁺-O2 bond lengths differ by 0.383 Å) lies 3.8 kJ/mol higher in energy than the ground-state conformer (where the M⁺-O1 and M⁺-O2 bond lengths are significantly different and differ by 1.537 Å). The M⁺-O1 bond distance is shorter in the M⁺(TEP) complexes than in the corresponding M⁺(TMP) complexes. The change in the C-O bond lengths

**Figure 6.** Bond dissociation energies at 0 K (in kJ/mol) of the M⁺-(TEP) complexes plotted vs the ionic radius of M⁺. All values are measured here by TCID and are taken from Table 3.**Figure 7.** Theoretical versus experimental 0 K M⁺-(TEP) bond dissociation energies (in kJ/mol), where M⁺ = Na⁺, K⁺, Rb⁺, and Cs⁺. All values are determined here and are taken from Table 3.

upon the alkali metal cation binding varies from 0.010 to 0.025 Å for the M⁺(TEP) complexes and is larger than that in the corresponding TMP complexes, 0.010–0.016 Å. The larger increase in the C-O bond lengths of the M⁺(TEP) complexes suggests that metal cations are able to activate TEP more readily than TMP.

TEP is found to bind the alkali metal cations (Na⁺, K⁺, Rb⁺, and Cs⁺) more strongly than TMP. The enhanced binding to TEP is likely the result of its larger size and therefore greater polarizability than TMP (16.42 \AA^3 versus 10.80 \AA^3),¹⁵ which should help to delocalize the positive charge on the metal cation more efficiently. The trends in the BDEs for the M⁺(TMP) and M⁺(TEP) complexes are similar and decrease monotonically as the size of alkali metal cation increases. No activated dissociation was observed for Na⁺, K⁺, Rb⁺, and Cs⁺ binding to TEP and TMP because the alkali metal cation-phosphate ester binding interactions in these complexes are purely non-covalent in nature and are weaker than the covalent bonds within these phosphate esters. Therefore, these alkali metal cations are probably not good candidates for activating the phosphodiester linkages of nucleic acids. However, the M⁺-TEP BDEs measured here can be used as reliable anchors for the alkali metal cation affinity scales.

The binding of Li⁺ to TEP is stronger and more covalent in nature than the larger alkali metal cations. Activated dissociation of the Li⁺(TEP) complex is observed upon CID with Xe. Therefore, the results for the Li⁺(TEP) complex are not included here but will be presented in detail in a future paper that examines the activation of TEP by various other metal cations. In contrast, no activated dissociation was observed for the Li⁺-(TMP) complex. This is consistent with the stronger binding

of Li⁺ to TEP than to TMP and also indicates that more energy is needed to activate TMP than TEP.

In biological systems, alkali metal cations bind nonspecifically to the phosphate groups along the backbone of nucleic acids. Their primary function is to neutralize the charges on the phosphate groups along the deprotonated backbone; they are generally not involved in catalytic processes. The simple electrostatic binding and CID behavior of complexes of the alkali metal cations with TMP and TEP found here and in our previous study¹⁵ is consistent with their behavior in biological systems.

Conclusions

The kinetic energy dependences of the CID of M⁺(TEP) complexes, where M⁺ = Na⁺, K⁺, Rb⁺, and Cs⁺, with Xe are examined in a guided ion beam tandem mass spectrometer. The dominant pathway observed for all complexes is loss of the intact TEP ligand. The thresholds for these dissociation processes are interpreted to yield 0 and 298 K M⁺–(TEP) BDEs. The molecular parameters needed for the analysis of experimental data as well as structures and theoretical estimates of the BDEs for the M⁺(TEP) complexes are obtained from theoretical calculations performed at the B3LYP/6-311+G(2d,-2p)//B3LYP/6-31G* and B3LYP/6-311+G(2d,2p), HW//B3LYP/6-31G*, HW levels of theory. The agreement between theory and experiment is excellent for the Na⁺ and K⁺ complexes and is somewhat less satisfactory for the Rb⁺ and Cs⁺ complexes. The poorer agreement found for the Rb⁺ and Cs⁺ complexes is probably the result of the effective core potentials used to describe these metal cations. The M⁺–(TEP) BDEs are observed to decrease monotonically as the size of the alkali metal cation increases from Na⁺ to Cs⁺. This trend is explained in terms of the electrostatic nature of the binding. The mode of alkali metal cation binding to TEP is very similar to that found for the analogous M⁺(TMP) complexes and involves the alkali metal cation interacting with the lone pairs of electrons on the oxo and one of the alkoxy oxygen atoms. The binding of alkali metal cations to TEP is stronger than to TMP and results in a more significant lengthening of the C–O bonds. No activated dissociation is observed upon CID for Na⁺, K⁺, Rb⁺, and Cs⁺ binding to TEP and TMP because of the purely noncovalent nature of the binding to these alkali metal cations.

Acknowledgment. This work is supported by the National Science Foundation, Grant CHE-0518262.

Supporting Information Available: Tables of vibrational frequencies, average vibrational energies at 298 K, rotational constants, and Cartesian coordinates of the B3LYP/6-31G* optimized geometries of TEP and M⁺(TEP) in their ground-state conformations and enthalpies and free energies of M⁺ binding to TEP; figures showing cross sections for the collision-induced dissociation of M⁺(TEP) with Xe as well as empirical fits to the M⁺ product channels, where M⁺ = K⁺, Rb⁺, and Cs⁺. This material is free of charge via the Internet at <http://pubs.acs.org>.

References and Notes

- Eichhorn, G. L.; Butzow, J. J. *Proc. Int. Symp. Biomol. Struct. Interact. Suppl. J. Biosci.* **1985**, *8*, 527.
- Eichhorn, G. L. *Metal Ions in Genetic Information Transfer*; Elsevier: New York, 1981.
- Sletten, E.; Froystein, N. A. *Metal Ions in Biological Systems*; Dekker: New York, 1996; p 397.
- Hud, N. V.; Fiegon, J. J. *Am. Chem. Soc.* **1997**, *119*, 5756.
- Hud, N. V.; Sklenar, V.; Feigon, J. J. *Mol. Biol.* **1999**, *286*, 651.
- Shui, X. Q.; McFail-Isom, L.; Hu, G. G.; Williams, L. D. *Biochemistry* **1998**, *37*, 8341.
- Tereshko, V.; Minasov, G.; Egli, M. *J. Am. Chem. Soc.* **1999**, *121*, 3590.
- Young, M. A.; Jayaram B.; Beveridge, D. L. *J. Am. Chem. Soc.* **1997**, *119*, 59.
- Cheatham, T. E.; Kollman, P. A. *Annu. Rev. Phys. Chem.* **2000**, *51*, 435.
- Howerton, S. B.; Sines, C. C.; Vanderveer, D.; Williams, L. D. *Biochemistry* **2001**, *40*, 10023.
- Eichhorn, G. L. *Advances in Inorganic Biochemistry*; Elsevier: New York, 1981; Vol. 3, p 2.
- Schneider, B.; Kabelac, M. *J. Am. Chem. Soc.* **1998**, *120*, 161.
- Schneider, B.; Kabelac, M.; Hobza, P. *J. Am. Chem. Soc.* **1996**, *118*, 161.
- Deerfield, D. W., II; Pedersen, L. G. *J. Biomol. Struct. Dyn.* **1995**, *13*, 167.
- Ruan, C.; Huang, H.; Rodgers, M. T. *J. Am. Soc. Mass Spectrom.* accepted for publication (JASMS-2007-3447).
- Rodgers, M. T.; Ervin, K. M.; Armentrout, P. B. *J. Chem. Phys.* **1997**, *106*, 4499.
- Rodgers, M. T. *J. Phys. Chem. A* **2001**, *105*, 2374.
- Teloy, E.; Gerlich, D. *Chem. Phys.* **1974**, *4*, 417.
- Gerlich, D. Diplomarbeit, University of Freiburg, Federal Republic of Germany, 1971.
- Gerlich, D. In *State-Selected and State-to-State Ion-Molecule Reaction Dynamics, Part I, Experiment*; Ng, C.-Y., Baer, M., Eds.; Advances in Chemical Physics Series; Wiley: New York, 1992; 82, p 1.
- Dalleska, N. F.; Honma, K.; Armentrout, P. B. *J. Am. Chem. Soc.* **1993**, *115*, 12125.
- Aristov, N.; Armentrout, P. B. *J. Phys. Chem.* **1986**, *90*, 5135.
- Hales, D. A.; Armentrout, P. B. *J. Cluster Sci.* **1990**, *1*, 127.
- Ervin, K. M.; Armentrout, P. B. *J. Chem. Phys.* **1985**, *83*, 166.
- Dalleska, N. F.; Honma, K.; Sunderlin, L. S.; Armentrout, P. B. *J. Am. Chem. Soc.* **1994**, *116*, 3519.
- Frisch, M. J.; Trucks, G. W.; Schlegel, H. B.; Scuseria, G. E.; Robb, M. A.; Cheeseman, J. R.; Montgomery, J. A., Jr.; Vreven, T.; Kudin, K. N.; Burant, J. C.; Millam, J. M.; Iyengar, S. S.; Tomasi, J.; Barone, V.; Mennucci, B.; Cossi, M.; Scalmani, G.; Rega, N.; Petersson, G. A.; Nakatsuji, H.; Hada, M.; Ehara, M.; Toyota, K.; Fukuda, R.; Hasegawa, J.; Ishida, M.; Nakajima, T.; Honda, Y.; Kitao, O.; Nakai, H.; Klene, M.; Li, X.; Knox, J. E.; Hratchian, H. P.; Cross, J. B.; Adamo, C.; Jaramillo, J.; Gomperts, R.; Stratmann, R. E.; Yazyev, O.; Austin, A. J.; Cammi, R.; Pomelli, C.; Ochterski, J. W.; Ayala, P. Y.; Morokuma, K.; Voth, G. A.; Salvador, P.; Dannenberg, J. J.; Zakrzewski, V. G.; Dapprich, S.; Daniels, A. D.; Strain, M. C.; Farkas, O.; Malick, D. K.; Rabuck, A. D.; Raghavachari, K.; Foresman, J. B.; Ortiz, J. V.; Cui, Q.; Baboul, A. G.; Clifford, S.; Cioslowski, J.; Stefanov, B. B.; Liu, G.; Liashenko, A.; Piskorz, P.; Komaromi, I.; Martin, R. L.; Fox, D. J.; Keith, T.; Al-Laham, M. A.; Peng, C. Y.; Nanayakkara, A.; Challacombe, M.; Gill, P. M. W.; Johnson, B.; Chen, W.; Wong, M. W.; Gonzalez, C.; Pople, J. A. *Gaussian 03, Revision C.01*; Gaussian, Inc.: Wallingford, CT, 2004.
- Hay, P. J.; Wadt, W. R. *J. Chem. Phys.* **1985**, *82*, 299.
- Glendening, E. D.; Feller, D.; Thompson, M. A. *J. Am. Chem. Soc.* **1994**, *116*, 10657.
- Boys, S. F.; Bernardi, R. *Mol. Phys.* **1979**, *19*, 553.
- van Duijneveldt, F. B.; van Duijneveldt-van de Rijdt, J. G. C. M.; van Lenthe, J. H. *Chem. Rev.* **1994**, *94*, 1873.
- Smith, S. M.; Markevitch, A. N.; Romanov, D. A.; Li, X.; Levis, R. J.; Schlegel, H. B. *J. Phys. Chem. A* **2000**, *108*, 11063.
- Muntean, F.; Armentrout, P. B. *J. Chem. Phys.* **2001**, *115*, 1213.
- Beyer, T. S.; Swinehart, D. F. *Comm. Assoc. Comput. Machines* **1973**, *16*, 379.
- Stein, S. E.; Rabinovitch, B. S. *J. Chem. Phys.* **1973**, *58*, 2438.
- Stein, S. E.; Rabinovitch, B. S. *Chem. Phys. Lett.* **1977**, *49*, 183.
- Khan, F. A.; Clemmer, D. E.; Schultz, R. H.; Armentrout, P. B. *J. Phys. Chem.* **1993**, *97*, 7978.
- Chesnavich, W. J.; Bowers, M. T. *J. Phys. Chem.* **1979**, *83*, 900.
- See, for example, Figure 1 in Dalleska, N. F.; Honma, K.; Armentrout, P. B. *J. Am. Chem. Soc.* **1993**, *115*, 12125.
- Armentrout, P. B.; Simons, J. *J. Am. Chem. Soc.* **1992**, *114*, 8627.
- Amunugama, R.; Rodgers, M. T. *J. Phys. Chem. A* **2002**, *106*, 5529.
- Amunugama, R.; Rodgers, M. T. *J. Phys. Chem. A* **2002**, *106*, 9092.
- Amunugama, R.; Rodgers, M. T. *J. Phys. Chem. A* **2002**, *106*, 9718.
- Amunugama, R.; Rodgers, M. T. *Int. J. Mass Spectrom.* **2003**, *222*, 431.
- Amunugama, R.; Rodgers, M. T. *Int. J. Mass Spectrom.* **2003**, *227*, 1.
- Amunugama, R.; Rodgers, M. T. *Int. J. Mass Spectrom.* **2003**, *227*, 339.
- Ruan, C.; Yang, Z.; Hallowita, N.; Rodgers, M. T. *J. Phys. Chem. A* **2005**, *109*, 11539.
- Ruan, C.; Yang, Z.; Rodgers, M. T. *Int. J. Mass Spectrom.* **2007**, *267*, 233.